TISSUE ENGINEERING: Part A
Volume 22, Numbers 11 and 12, 2016

DOI: 10.1089/ten.tea.2015.0230

termis
Tissue Engineering
& Regenerative Medicine
International Society

ORIGINAL ARTICLE

Vertebral Implantation of NELL-1 Enhances Bone Formation in an Osteoporotic Sheep Model

Aaron W. James, MD,[1–3,*] Michael Chiang, BDS,[2,*] Greg Asatrian, BS,[2,*] Jia Shen, PhD,[1,2] Raghav Goyal, BS,[2] Choon G. Chung, DDS,[2] Le Chang, BS,[1,2] Swati Shrestha, BS,[1,2] A. Simon Turner, BVSc, MS, DVSc,[4] Howard B. Seim III, DVM, DVSc,[4] Xinli Zhang, MD, PhD,[1,2] Benjamin M. Wu, DDS, PhD,[5] Kang Ting, DMD, DMedSci,[1,2] and Chia Soo, MD, FACS[1,6]

Background: Vertebral compression fractures related to osteoporosis greatly afflict the aging population. One of the most commonly used therapy today is balloon kyphoplasty. However, this treatment is far from ideal and is associated with significant side effects. NELL-1, an osteoinductive factor that possesses both pro-osteogenic and anti-osteoclastic properties, is a promising candidate for an alternative to current treatment modalities. This study utilizes the pro-osteogenic properties of recombinant human NELL-1 (rhNELL-1) in lumbar spine vertebral defect model in osteoporotic sheep.

Methods: Osteoporosis was induced through ovariectomy, dietary depletion of calcium and vitamin D, and steroid administration. After osteoporotic induction, lumbar vertebral body defect creation was performed. Sheep were randomly implanted with the control vehicle, comprised of hyaluronic acid (HA) with hydroxyapatite-coated β-tricalcium phosphate (β-TCP), or the treatment material of rhNELL-1 protein lyophilized onto β-TCP mixed with HA. Analysis of lumbar spine defect healing was performed by radiographic, histologic, and computer-simulated biomechanical testing.

Results: rhNELL-1 treatment significantly increased lumbar spine bone formation, as determined by bone mineral density, % bone volume, and mean cortical width as assessed by micro-computed tomography. Histological analysis revealed a significant increase in bone area and osteoblast number and decrease in osteoclast number around the implant site. Computer-simulated biomechanical analysis of trabecular bone demonstrated that rhNELL-1-treatment resulted in a significantly more stress-resistant composition.

Conclusion: Our findings suggest rhNELL-1-based vertebral implantation successfully improved cortical and cancellous bone regeneration in the lumbar spine of osteoporotic sheep. rhNELL-1-based bone graft substitutes represent a potential new local therapy.

Introduction

Osteoporosis is the most common disease of bone, responsible for ~700,000 vertebral compression fractures (VCFs) in the United States annually.[1] When untreated, VCF can cause debilitating back pain, spinal deformity, disability, reduction of respiratory function, and a higher risk of death.[2–6] The annual cost of osteoporotic fractures in the United States is estimated to be at least $5–10 billion.[1] Due to an aging United States and world population, annual costs for osteoporotic fractures are projected to increase four-fold by 2040.[1]

In simplistic terms, age-related bone loss results from diminished bone formation and inappropriate bone resorption. In addition, aging increases the number of mesenchymal marrow stem cells (MSC)-derived adipocytes and decreases the number of MSC-derived osteoblasts.[7] These create

[1]Departments of Surgery and Orthopaedic Surgery, Orthopaedic Hospital Research Center, UCLA and Orthopedic Hospital, Los Angeles, California.
[2]Division of Growth and Development and Section of Orthodontics, Dental and Craniofacial Research Institute, School of Dentistry, University of California, Los Angeles, Los Angeles, California.
[3]Department of Pathology and Laboratory Medicine, University of California, Los Angeles, Los Angeles, California.
[4]Department of Veterinary Sciences, Colorado State University, Fort Collins, Colorado.
[5]Departments of Bioengineering and Material Sciences, University of California, Los Angeles, Los Angeles, California.
[6]Division of Plastic and Reconstructive Surgery, Department of Surgery, David Geffen School of Medicine, University of California, Los Angeles, Los Angeles, California.
*The indicated authors share equal responsibility for the work presented herein.

unfavorable conditions for bone stem cell participation in fracture repair and commonly lead to failure in healing osteoporotic fractures.[8] Consequently, it is crucial to investigate methods to prevent and heal VCF in osteoporotic patients.

Balloon kyphoplasty is a procedure performed to relieve back pain, increase function, and improve quality of life after VCF.[9] Kyphoplasty involves the inflation of a balloon in the vertebral body, followed by the injection of cement such as polymethyl methacrylate (PMMA) into the space created by the balloon.[10] From recent studies, balloon kyphoplasty with PMMA results in significant improvements in patients' quality of life, functionality, and overall reduction in pain in comparison to nonsurgical treatments.[11,12] For example, studies have shown patients treated with balloon kyphoplasty have increased vertebral height, functional capacities, and a significant improvement in Visual Analog Scale pain measurements.[12] However, current PMMA cement-based VCF therapies have significant disadvantages including cellular toxicity and potential for neural damage caused by an acute exothermic reaction during polymerization of the PMMA.[13]

Besides potential for high local toxicity, cement from the fracture site can leak, and in rare cases cause embolization and death.[14] In addition, long-term complications can arise due to differences in the stiffness of cement and bone, predisposing the patient to adjacent fractures or re-fractures of the cement-treated vertebrae.[15] Moreover, PMMA cement-based VCF therapies may permanently exclude and eliminate MSC from the vertebral bone marrow space due to cellular toxicity, thus hampering endogenous bone healing. Due to the safety concerns of PMMA cements, calcium phosphate cement (CPC) has been used as an alternative. However, CPC induces ectopic bone formation,[16] and heterotopic ossification, which alters the normal biomechanics and results in subsequent VCFs.[17]

Nel-like molecule-1 (NELL-1) is a novel osteogenic differentiation factor, first identified to have osteoinductive properties by its overexpression in craniosynostosis patients.[18] NELL-1 is a secreted protein comprised of 810 amino acids.[18] NELL-1 contains several structural motifs, including a secretory signal peptide, a thrombospondin-1 (TSP-1)-like module (TSPN, overlapping with a laminin G domain), four chordin-like, cysteine-rich (CR) domains, and six epidermal growth factor (EGF)-like domains.[18] NELL-1 stimulates bone regeneration via either endochondral or intramembranous ossification.[18] In addition, previous studies have demonstrated the ability of NELL-1 to induce significant bone formation in calvarial, axial, and appendicular defects, in both small and large animal models.[19–23]

Currently, bone morphogenetic protein 2 (BMP2) is the gold standard substitute for autogenous bone, and although causing significant bone formation, it is also associated with multiple clinical complications such as soft-tissue swelling, ectopic bone formation, and inflammation.[24–31] In contrast, NELL-1 is an osteoblast-specific growth factor, and suppresses the BMP2-induced side effects of cystic bone formation[32] and inflammation.[33] Moreover, NELL-1 directly represses adipogenic differentiation[34] and osteoclastogenesis.[35] Mechanistically, NELL-1 is known to have multiple effects including regulation of Runt-related transcription factor-2 (Runx2) activity and phosphorylation,[36] positive regulation of MAPK,[37] Hedgehog,[34] and Wnt signaling.[35]

In this study, we investigate the therapeutic effects of recombinant human NELL-1 (rhNELL-1) in an osteoporotic sheep model by evaluating healing of lumbar spine defects after vertebral body implantation of rhNELL-1. Sheep were used as they have similarities to humans in terms of spinal dimensions in addition to mineral and collagen composition.[38] The sheep model is optimal because their vertebral bodies are large enough to accommodate a large volume defect.[39] Additionally, sheep are susceptible to osteoporosis with a combined treatment of ovariectomy, steroid administration, and dietary deficiency.[39] In fact, after a 4-month induction period, sheep show resemblance to postmenopausal osteoporotic women.[39] Briefly, we found rhNELL-1 vertebral body implantation successfully induced an increase in osteoblast and a decrease in osteoclast activity resulting in improved cortical and cancellous bone formation in osteoporotic sheep spine.

Materials and Methods

Animal care and ovine osteoporotic induction

Sheep were cared for at Colorado State University according to the Guiding Principles in the Care and Use of Animals. Osteoporosis in 4-year-old sheep was induced through ovariectomy (OVX), dietary depletion, and steroid administration in eight adult ewes. Mean animal body weight was 75 kg (standard deviation: 9.1 kg). Average height was 89 cm at withers and 122 cm from nose to tail. OVX was performed as previously described.[40] Three intramuscular injections of 500 mg methylprednisolone acetate (Depomedrol) were administered at 3-week intervals starting 2 weeks post-OVX. Specifically formulated low calcium and low vitamin D osteoporosis diets (Purina LabDiet) were fed to the sheep for the entire study period.[41] Of eight sheep, six with highest response to osteoporotic induction were used for further study. Response to osteoporotic induction was evaluated by dual-energy X-ray absorptiometry (DXA). A timeline of the study structure including osteoporotic induction, vertebral implantation, and postoperative analyses can be found in Figure 1A.

rhNELL-1 implant material preparation

The contents of sheep implant material can be found in Supplementary Figure S1 (Supplementary Data are available online at www.liebertpub.com/tea). NELL-1 implant dosages were used as previously described.[23,35] The control implant material was composed of hyaluronic acid (HA, 1.5 mL) and hydroxyapatite-coated β-tricalcium phosphate (β-TCP; 150 mg, granule size: 50 μm, pore size: 10 μm, mixed with 500 μm hydroxyapatite). β-TCP has been previously shown to increase the biochemical stability and biological efficiency of rhNELL-1 *in vivo*.[42] Hydroxyapatite coating was performed as previously described.[43] The treatment implant materials consisted of two dosages of rhNELL-1 protein lyophilized onto β-TCP mixed into the HA, for sustained protein release.[20] The individual components were mixed mechanically before implantation.

Ovine rhNELL-1 implantation

Surgery was performed 4 months post-OVX on $n=6$ osteoporotic sheep (those six sheep most responsive to

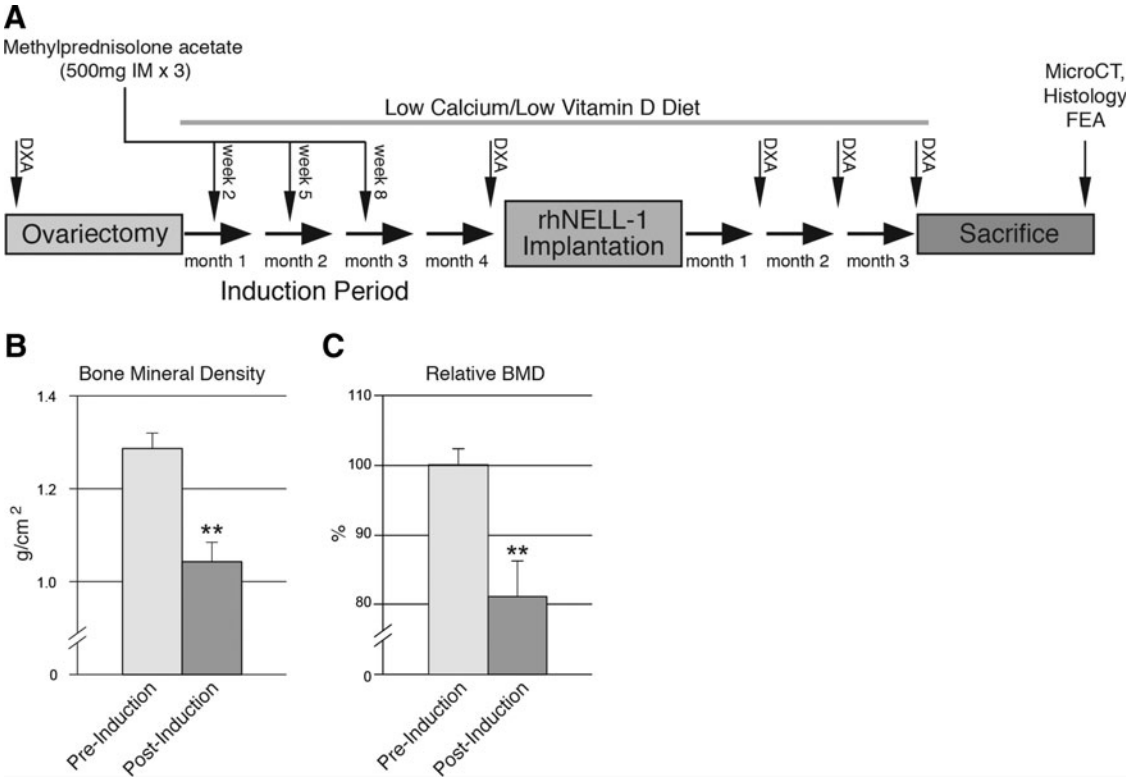

FIG. 1. Induction of osteoporosis in sheep. **(A)** Timeline of osteoporosis induction in sheep. Osteoporosis was induced by combination of treatment with ovariectomy, steroid injection, and low calcium/low vitamin D diet. Pre- and postinduction DXA scans were performed. Postimplantation of rhNELL-1 treatment materials, DXA scans were performed monthly until sacrifice at 3 months, after which microCT, histological analysis, and finite element analysis (FEA) were performed. **(B,C)** DXA imaging performed postinduction showed a significant decrease in bone mineral density (BMD) within the sheep lumbar spine from 0 to 4 months. Data derived from $n=6$ with sheep most responsive to osteoporotic induction used for subsequent experimentation, with $n=8$ sheep in total. DXA, dual-energy X-ray absorptiometry; microCT, micro-computed tomography; rhNELL-1, recombinant human NELL-1. $^{**}P<0.01$.

induction). A ventrolateral incision was made for a retroperitoneal approach. Dissection was carried out to expose the cranial aspect of the lumbar vertebral bodies. Two different vertebral levels were instrumented per sheep (L2 and L4). A 6.0 mm diameter access hole was first drilled in the lateral aspect of the vertebral body. With a Midas Rex bur, a 2.0 cm diameter defect was then created in the central portion of the vertebral body. Next, the knitted OptiMesh® implant sac (Spineology) was inserted into the vertebral defect (Supplementary Fig. S2). The rhNELL-1 test article was delivered into the mesh bag by impacting a stylet down into the central core with a mallet. Finally, the access hole was covered with bone wax, to prevent leakage. $n=3$ sheep were randomly assigned to implantation with the control vehicle and $n=3$ sheep with the treatment.

Live ovine radiographic analysis

DXA scans were acquired pre- and postinduction of osteoporosis, and monthly postimplantation (Konica Minolta mc5430DL). Bone mineral density (BMD) was measured as a result of bone mineral content (g)/area (cm^2).

Postmortem micro-computed tomography

High resolution, postmortem micro-computed tomography (microCT) scanning and analysis were performed on individual sheep vertebrae. Samples were surgically harvested and placed in 10% formalin in phosphate buffered saline (PBS) for fixation. Samples were imaged using high-resolution microCT (Skyscan 1172F; Skyscan) at an image resolution of 17.8–18.2 μm and analyzed using Data Viewer, Recon, CTAn, and CTVol softwares provided by the manufacturer. Cortical and trabecular analyses were performed on postmortem individual sheep vertebrae. Cortical measurements were obtained per vertebral body, either assessing the cortex through which the implant was placed or the opposing cortex. Trabecular measurements were made using region of interests (ROIs) encompassing the entire cancellous bone using CTAn software. All quantitative and structural morphometric data use nomenclature described by the American Society for Bone and Mineral Research (ASBMR) Nomenclature Committee.[44]

Histological and histomorphometric analyses

After radiographic analysis, undecalcified histological preparations were performed. Five micrometers thick sections were stained with hematoxylin and eosin, Goldner's modified trichrome (GMT), and Von Kossa–MacNeal's Tetrachrome. Histologic specimens were analyzed using Olympus BX51 microscopes and images were obtained using MicroFire digital camera with Picture Frame software (Optronics). Histomorphometric analysis was completed

using Adobe Photoshop. For cortical bone, $n=12$ random contralateral side fields of implantation were used for analysis. For trabecular bone, three random fields from each specimen were used for analysis (equating to $n=18$ images for control samples and $n=9$ images for each NELL-1 treatment group). Measurements included percent Trabeculae Area (% Tb. Ar), Cortical Width (Ct. Wi), Trabecular Width (Tb. Wi), Trabecular Number (Tb. N), and Trabecular Spacing (Tb. Sp). Cortical Width was measured on the contralateral side of product implantation. Osteoblast Number (Ob. N) was measured using 200× images of Von Kossa–McNeal's Tetrachrome-stained specimens, whereas Osteoclast Number (Oc. N) was measured using 200× images of GMT staining. All quantitative and structural morphometric data use nomenclature described by the ASBMR Nomenclature Committee.[45]

Finite element analysis

To simulate the biomechanical properties of newly formed trabecular bone, microCT images were converted to DICOM files using SkyScan Dicom Converter software. Tetrahedral three-dimensional mesh models were created using ScanIP software (Simpleware Limited) by drawing a ROI 0.5 mm caudal to the implant site in the midline of the vertebra spanning $5\times5\times10$ mm. Finite element analysis (FEA) was performed using ABAQUS software (Dassault Systèmes). Boundary conditions were set as encastre, constrained in all directions on the lower (caudal) border nodes of the hexahedron. Since similar biomechanical properties are shared between human and sheep vertebral bodies,[45] we applied a uniform compressive stress of 0.5 MPa on the superior surface of the spine, to reproduce human intradiscal pressure experienced in relaxed standing. Finally, the resulting strain energy and tensile strength were analyzed.[46]

Statistical analysis

Quantitative data are expressed at mean ± SEM unless otherwise described, with $*p<0.05$ and $**p<0.01$ considered significant. A Shapiro–Wilk test for normality was performed on all datasets. Homogeneity was confirmed by a comparison of variances test. Parametric data were analyzed using an appropriate Student's *t*-test when two groups were being compared, or a one-way analysis of variance was used when more than two groups were compared, followed by a *post-hoc* Tukey's test to compare two groups. Nonparametric data were analyzed with a Mann–Whitney *U* test when two groups were being compared or a Kruskal–Wallis one-way analysis when more than two groups were compared.

Results

DXA analysis

Osteoporosis was induced over a 4 month period through ovariectomy, dietary deficiency, and steroid administration (Fig. 1A). To verify successful induction, DXA scans were performed pre- and postinduction, and demonstrated a significant decrease in BMD within the lumbar spine (Fig. 1B). Next, vertebral implantation was performed in the six sheep most susceptible to induction (those with greatest loss of BMD). Sheep were randomly implanted with the control vehicle, comprised of HA and β-TCP or rhNELL-1 protein lyophilized onto β-TCP mixed with HA (Supplementary Fig. S1). Two doses of rhNELL-1 were used (0.9 and 2.25 mg). Animals next underwent monthly DXA for 3 months. Results showed that rhNELL-1 treatment with either 0.9 or 2.25 mg exhibited a significant increase in BMD in comparison to control (Fig. 2). A statistically significant difference was most apparent at 2 months postoperative ($*p=0.027$, $**p=0.007$). At 3 months postoperative, a persistent increase in BMD was appreciated at the higher dose of 2.25 mg rhNELL-1 treatment ($*p=0.047$). In summary, analysis of DXA scans showed a significant increase in BMD among rhNELL-1-based implantation specimens in comparison to control.

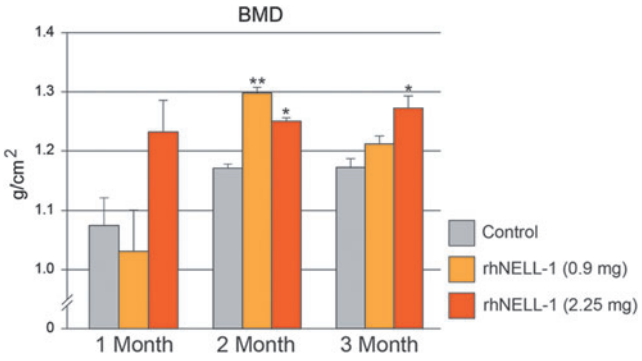

FIG. 2. BMD quantification in sheep lumbar vertebrae. DXA Scans were performed at 1, 2, and 3 months after vertebral implantation. Quantification of BMD between control, rhNELL-1 (0.9 mg), and rhNELL-1 (2.25 mg) groups was performed. DXA scans showed a significant increase in BMD with rhNELL-1-based implantation in comparison to control treatment. $n=3$ lumbar vertebrae per dose rhNELL-1, $n=6$ control-treated lumbar vertebrae. $n=6$ sheep in total. $*p<0.05$, $**p<0.01$ in comparison to control at corresponding time point. Color images available online at www.liebertpub.com/tea

MicroCT analysis

We next sought to delineate the effects of rhNELl-1 on either cortical or cancellous bone using high-resolution microCT scans. This allowed for the high-resolution analysis of three-dimensional trabecular bone structure. Axial and sagittal images of microCT scans showed significant bone formation particularly in rhNELL-1-based implantation groups (Fig. 3A). Trabecular bone analyses were performed, and showed a significant dose-dependent increase in BMD with rhNELL-1 treatment when compared to control (Fig. 3B). Next, percentage bone volume (BV/TV) was calculated, showing a significant increase with rhNELL-1 treatment at both 0.9 and 2.25 mg dosages (Fig. 3C). Although there was no significant difference in Trabecular Thickness (Tb. Th) (Fig. 3D) between treatment groups and control, a significant increase was observed in the Trabecular Number (Tb. N) of rhNELL-1 both treated groups (0.9 and 2.25 mg) (Fig. 3E). Additionally, a significant, dose-dependent decrease in Trabecular Spacing (Tb. Sp) was observed when comparing the rhNELL-1-treated treatment groups to control (Fig. 3F). In summary, microCT analysis exhibited a significant and dose-dependent increase in bone and trabecular bone quantitative measurements.

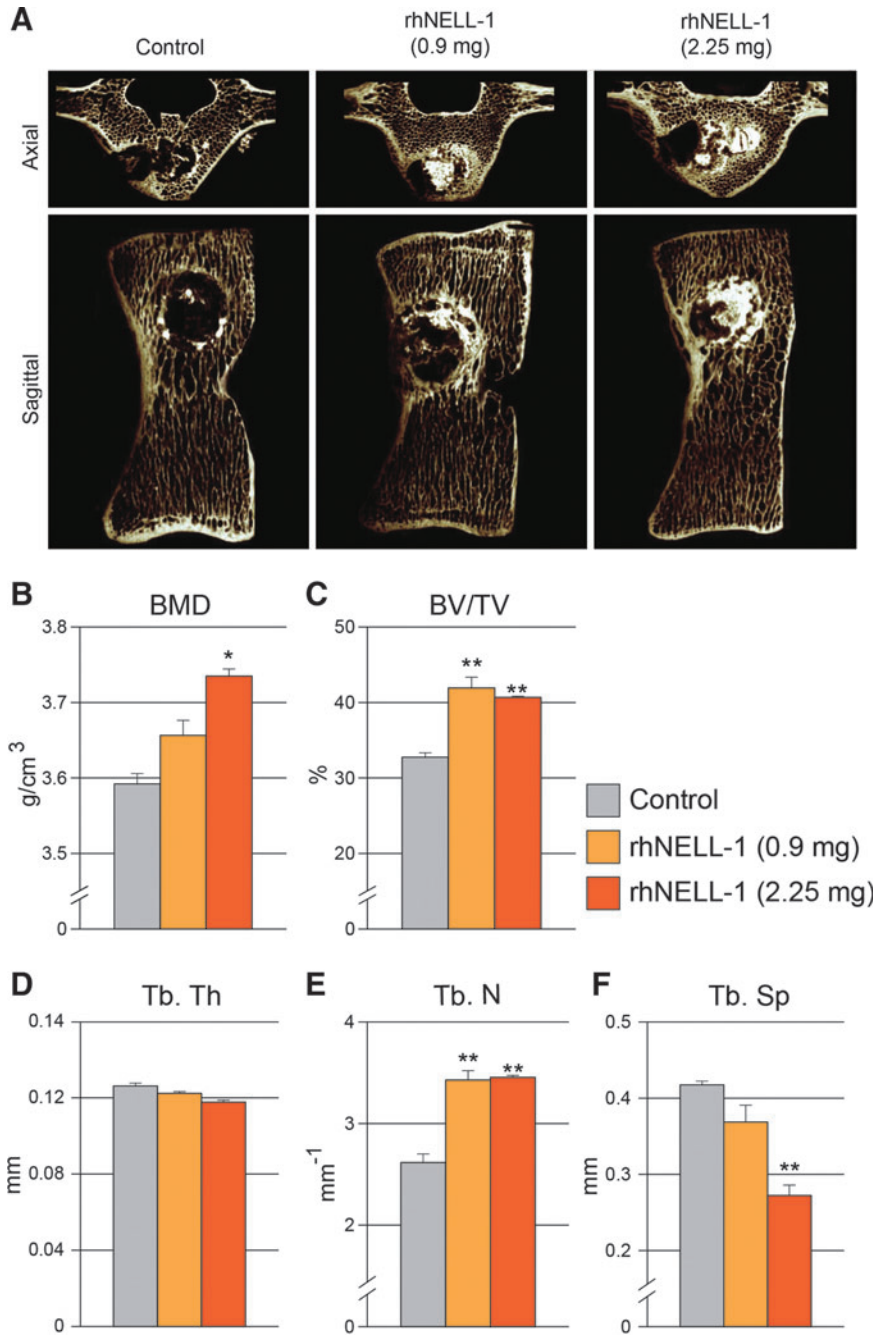

FIG. 3. MicroCT analysis of sheep lumbar vertebrae. **(A)** Representative microCT axial and sagittal reconstructions of sheep vertebrae treated with control, rhNELL-1 (0.9 mg) and rhNELL-1 (2.25 mg)-based implantation. After 3 months, microCT analysis was performed, including **(B)** BMD, **(C)** percentage bone volume (BV/TV), **(D–F)** trabecular bone measurements including, **(D)** Trabecular Thickness (Tb. Th), **(E)** Trabecular Number (Tb. N), and **(F)** Trabecular Spacing (Tb. Sp). $n=3$ lumbar vertebrae per dose rhNELL-1, $n=6$ control-treated lumbar vertebrae. $n=6$ sheep in total. $^{*}p<0.05$, $^{**}p<0.01$ in comparison to control. Color images available online at www.liebertpub.com/tea

Histological and histomorphometric analyses

Next, histology was performed on serial sections of implant sites to expand on radiographic findings. As shown by radiographic analysis, it was also observed that spines treated with rhNELL-1 exhibited a significant and dose-dependent increase in bone formation in comparison to vehicle control implantation. Von Kossa–MacNeal's Tetrachrome staining of the implant sites also demonstrated an increase in cancellous bone formation, appearing black, in comparison to the control (Fig. 4A). Histomorphometric analysis further reinforced the observed significant differences in bone formation. First, Cortical Width (Ct. Wi) quantifications of serial sections documented a significant and dose-dependent increase between rhNELL-1-treated groups in comparison to control. In both dosages, the rhNELL-1-treated group exhibited greater and thicker endocortical bone formation than the control treated group (Fig. 4B). Next, cancellous bone was analyzed. Both rhNELL-1-treated groups exhibited a greater percentage of Trabecular Bone Area (% Tb. Ar) in comparison to the control group (Fig. 4C). However, there was no significant difference in Trabecular Width (Tb. Wi) between treatment and control groups (Fig. 4D). When comparing Trabecular Number (Tb. N), a significant increase was observed between rhNELL-1-treated groups in comparison to the control (Fig. 4E).

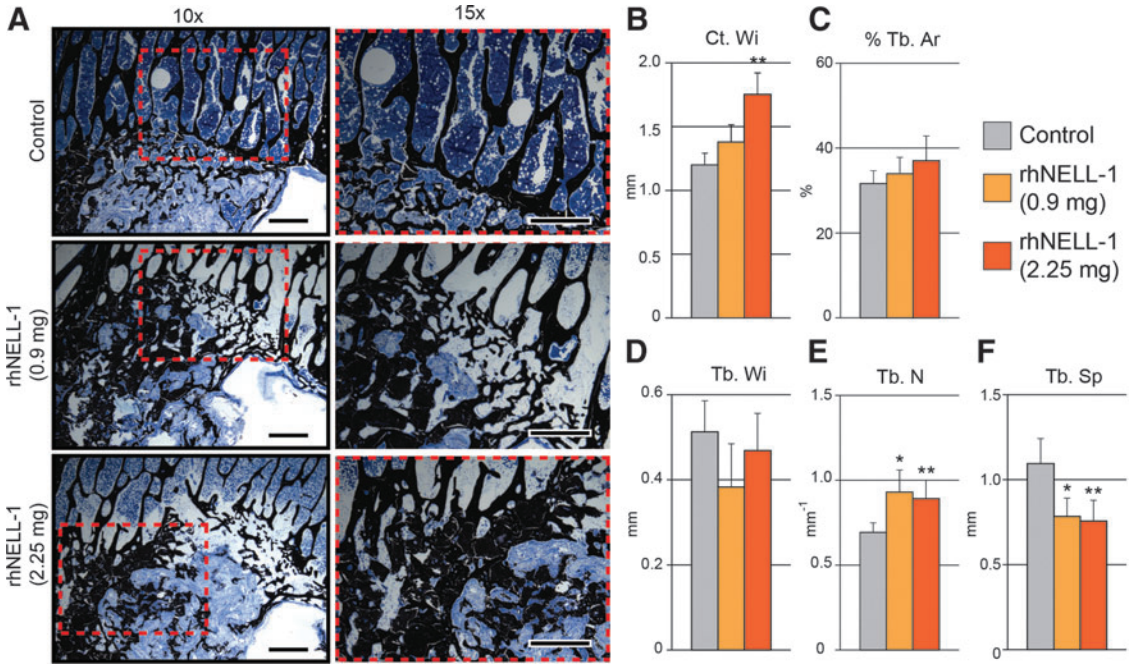

FIG. 4. Histological analysis of sheep lumbar vertebrae. **(A)** Representative images of Von Kossa–McNeal's Tetrachrome staining of sheep lumbar vertebral bodies were taken at peri-implant sites treated with control, rhNELL-1 (0.9 mg) and rhNELL-1 (2.25 mg). **(B–F)** Histomorphometric quantification using Von Kossa–McNeal's Tetrachrome stained slides of samples treated with control, rhNELL-1 (0.9 mg) and rhNELL-1 (2.25 mg)-based vertebral body implantation. Bone measurements include **(B)** Cortical Width (Ct. Wi), **(C)** Percent Trabecular Bone (% Tb. Ar), **(D)** Trabecular Width (Tb. Wi), **(E)** Trabecular Number (Tb. N), and **(F)** Trabecular Bone Spacing (Tb. Sp). $n=3$ lumbar vertebrae per dose rhNELL-1, $n=6$ control-treated lumbar vertebrae. $n=6$ sheep in total. $^{*}p<0.05$ and $^{**}p<0.01$ in comparison to control. Scale bar: 100 um. Color images available online at www.liebertpub.com/tea

Finally, a significant and dose-dependent decrease in Trabecular Spacing (Tb. Sp) was observed, suggesting dense cancellous bone formation with rhNELL-1 treatment (Fig. 4F). Thus, histomorphometric measurements served to confirm initial finding radiographic findings.

Increased trabecular bone with rhNELL-1 could be due to increased bone formation, reduced bone resorption, or a combination of the two processes. To evaluate this, we next examined osteoblasts and osteoclasts through histological analysis. Osteoblasts and Osteoclast Number were quantified

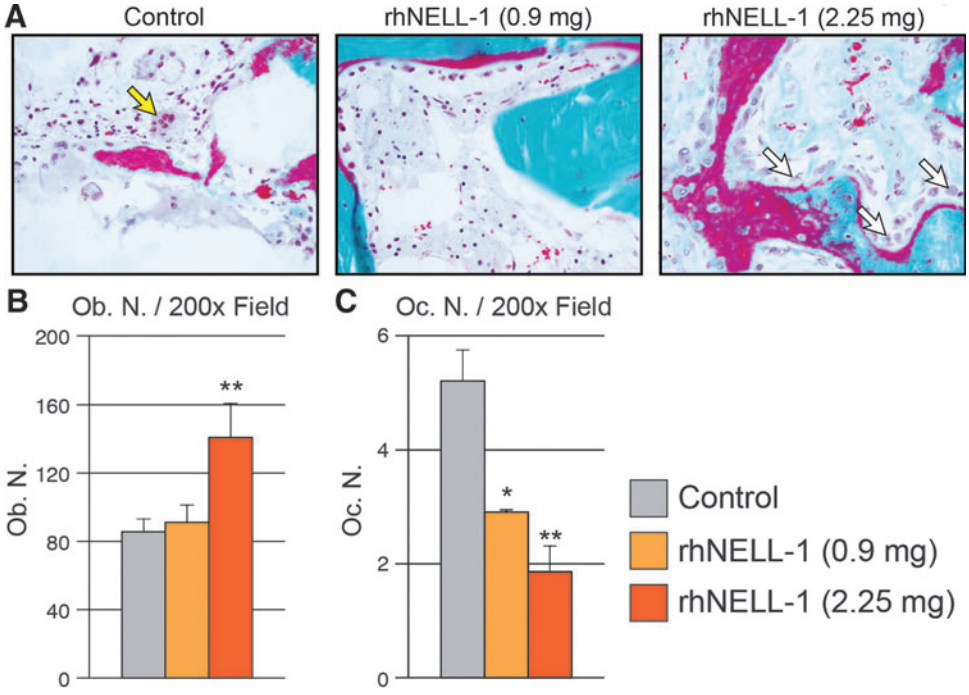

FIG. 5. Osteoblast and Osteoclast numbers in the peri-implant bone tissue. **(A)** Representative Goldner's modified trichrome staining demonstrating an increased osteoclast number in control-treated samples (*yellow arrow*) and osteoblasts in NELL-1-treated samples (*white arrow*). **(B)** Quantification of Osteoblast Number obtained from random histological fields (Ob. N/200× field). **(C)** Quantification of Osteoclast Number obtained from random histological fields (Oc. N/200× field). $n=3$ lumbar vertebrae per dose rhNELL-1, $n=6$ control-treated lumbar vertebrae. $n=6$ sheep in total. $^{*}p<0.05$, $^{**}p<0.01$ in comparison to control. Color images available online at www.liebertpub.com/tea

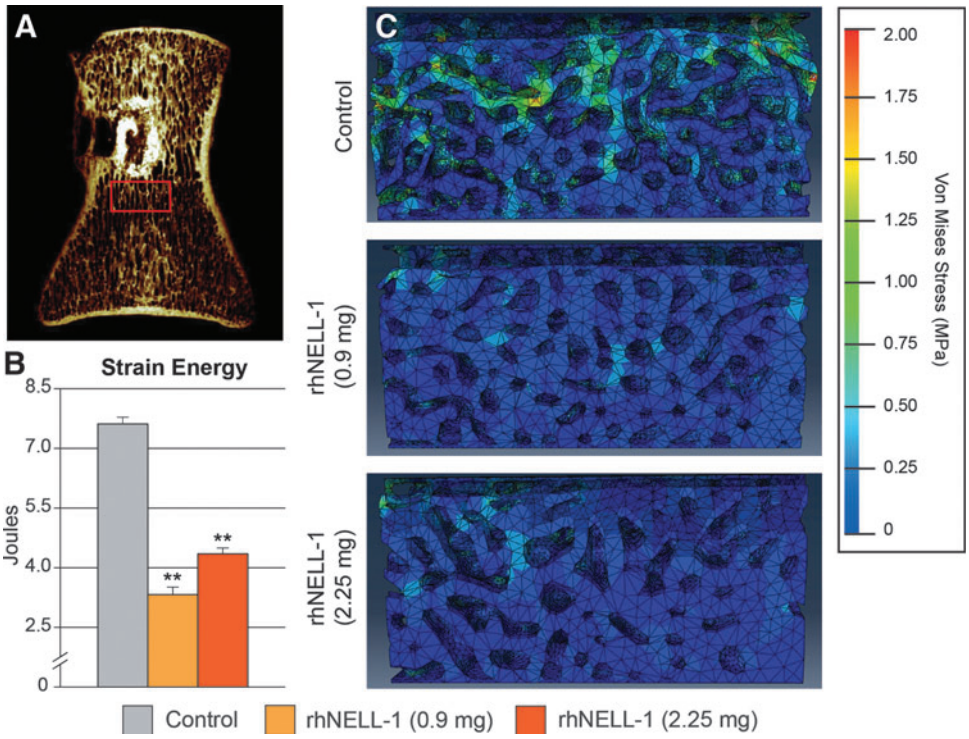

FIG. 6. FEA of peri-implant trabecular bone. **(A)** Region of interest (ROI) for biomechanical testing using FEA. A coronal microCT recontruction image shows the the area of trabecular bone positioned 0.5 mm caudal to the implant site in the midline of the vertebrae and spanning a $5 \times 10 \times 5$ mm ROI. **(B)** Total strain energy determined by FEA. **(C)** Representative images of FEA models showing stressed elements postloading. High strain areas are indicated with *yellow/green*. $n = 3$ lumbar vertebrae per dose rhNELL-1, $n = 6$ control-treated lumbar vertebrae. $n = 6$ sheep in total. $^{*}p < 0.05$, $^{**}p < 0.01$ in comparison to control. Color images available online at www.liebertpub.com/tea

in the peri-implant site tissue by examining cells for characteristic morphology (Fig. 5). Results showed that Osteoblast Number (Ob. N) per 200× field was significantly increased in the high dose rhNELL-1 group (Fig. 5A). Osteoblast number was determined by characteristic cuboidal morphology in bone-lining cells. In contrast, Osteoclast Number (Oc. N) per 200× field showed a significant and dose-dependent decrease with rhNELL-1 treatment groups (Fig. 5B). Osteoclast number was defined as the number of tartrate-resistant acid phosphatase (TRAP) positive, multi-nucleated, bone-lining cells. In summary, rhNELL-1 treatment resulted in a dose-dependent increase in bone formation, including endocortical and cancellous bone. This was accompanied by an increase ratio of Osteoblast: Osteoclast cell number.

Computer simulated biomechanical analysis

Finally, computer-simulated biomechanical analysis was performed using FEA. This revealed decreased strain energy among rhNELL-1 treatment groups in comparison to control. A significant decrease in total strain energy was observed across both rhNELL-1 treatment groups in comparison to control (Fig. 6B). Compressive stress values of treatment groups were then visualized (Fig. 6C). Specimens with rhNELL-1 treatment exhibited similar compressive stress strains, ranging from 0.1 MPa (blue) to 0.5 MPa (cyan). This was compared to relatively higher compressive stress strain levels in the control group, ranging from 0.1 MPa (blue) to 1.5 MPa (green). In summary, FEA demonstrated that rhNELL-1-based implantation resulted in a more stress-resistant composition in comparison to control.

Discussion

In this study, our findings suggest that exogenous rhNELL-1 protein application via vertebral implantation led to an improvement in bone quality in osteoporotic sheep model, as evaluated by radiographic, histological, and biomechanical analyses. rhNELL-1 treatment was found to increase both cortical and cancellous bone in the lumbar vertebrae. FEA suggested an increase in the structural stability and resistance to compressive stress with rhNELL-1 treatment. Finally, an increase in the ratio of osteoblasts to osteoclasts was observed with rhNELL-1 delivery. This evidence demonstrated that rhNELL-1 plays a role as an anabolic and anti-osteoclastic agent for improved bone quantity and bone quality.

On a cellular level, osteoporosis can be attributed to the imbalance between bone formation and bone resorption.[47] This occurs due to a reduction in osteoblast number and activity, and an increase in osteoclast number and activity.[48] NELL-1 has previously been published suggesting its role as a positive regulator of osteoblastogenesis and bone deposition via Runx2 and MAPK signaling pathways. NELL-1 operates as a downstream mediator of Runx2, a key factor in osteogenic differentiation, and the upregulation of Runx2 via NELL-1 occurs by enhancement of its phosphorylation through activation of MAPK signaling.[37] However, the exact mechanisms for NELL-1's negative effects on bone resorption have yet to be fully understood. One possibility for this is via the canonical Wnt signaling pathway, which is known to enhance osteoprogenitor cell proliferation and osteoblastogenesis while also having antiosteoclast activity.[49] Ongoing studies are examining the potential intersection between NELL-1 and Wnt-signaling. Nonetheless, NELL-1 has promising results at combating osteoporosis by decreasing bone resorption and increasing bone formation.

This study's main implication is that rhNELL-1 may be a new potentially preferable bone graft substitute, and more importantly, a promising efficacious therapy in the setting of osteoporosis. Presently, therapeutic options for osteoporotic

patients are limited to bone grafts or PMMA balloon kyphoplasty. Autologous bone grafting remains the gold standard for bone repair,[50] though possessing significant disadvantages, including donor site morbidity,[51] complications due to extended operating time and limited supply of host bone.[52] To combat these issues, growth factor-based therapies were studied, of which the only FDA approved one is BMP2 (INFUSE® Bone Graft). Although showing promising osteoinductive properties, BMP2 acts as a direct stimulant of osteoclastic bone resorption,[53] which can lead to complications such as vertebral collapse or additional fractures. Thus, caution must be exercised when implementing BMP2-based therapies.

Alternately, PMMA balloon kyphoplasty has been increasingly adopted for the treatment of osteoporotic compression fracture.[54] However, as mentioned PMMA has several associated potential risks. PMMA is not bioabsorbable and its unreacted monomer is toxic. Additionally, it has high polymerization temperatures[13] and its high stiffness causes a biomechanical mismatch between treated and untreated vertebral levels, leading to adjacent-level fractures.[15] In contrast, no previous studies have reported NELL-1 to be toxic or have any other associated adverse effects. Finally, rhNELL-1 lyophilized on a porous and resorbable β-TCP scaffold with hydroxyapatite coating allows better interaction with host bone. It increases both, the biochemical stability and the bioavailability of rhNELL-1 for protein delivery.[43] Together with our results, rhNELL-1 is a promising future component of a bone graft substitute for treatment in the setting of osteoporosis.

In summary, we have found that treatment with implantation of rhNELL-1 prevented further resorption of bone and increased regeneration of bone in the setting of osteoporosis in sheep. rhNELL-1 vertebral body implantation successfully induced an increase in osteoblast number and conversely a decrease in osteoclast number resulting in improved cortical and cancellous bone regeneration in osteoporotic sheep spine. Therefore, local rhNELL-1 treatment represents a potential new anabolic, anti-resorptive local therapy for treating osteoporotic bone loss and/or fractures.

Acknowledgments

This work was supported by NIH/NIAMS (grants R01 AR066782-01, AR068835-01A1, AR061399-01A1, K08 AR068316-01), UCLA/NIH CTSI grant UL1TR000124, National Aeronautical and Space Adminstration ''NASA'' GA-2014-154, the UCLA Department of Pathology and Laboratory Medicine, and the Translational Research Fund, the UCLA Daljit S. and Elaine Sarkaria Fellowship award, the Orthopedic Research and Education Foundation with funding provided by the Musculoskeletal Transplant Foundation, and T32 training fellowship (5T32DE007296-14) to A.W.J. The authors thank Ms. Nguyen and Giacomelli for their excellent technical assistance.

Disclosure Statement

Drs. X.Z., B.M.W., K.T., and C.S. are inventors of NELL-1-related patents. Drs. X.Z., B.M.W., K.T., and C.S. are founders and/or board members of Bone Biologics Inc., which sublicenses NELL-1 patents from the UC Regents, which also hold equity in the company.

References

1. Riggs, B.L., and Melton, L.J., 3rd. The worldwide problem of osteoporosis: insights afforded by epidemiology. Bone **17,** 505S, 1995.
2. Leidig, G., Minne, H.W., Sauer, P., Wuster, C., Wuster, J., Lojen, M., Raue, F., and Ziegler, R. A study of complaints and their relation to vertebral destruction in patients with osteoporosis. Bone Miner **8,** 217, 1990.
3. Mathis, J.M., Petri, M., and Naff, N. Percutaneous vertebroplasty treatment of steroid-induced osteoporotic compression fractures. Arthritis Rheum **41,** 171, 1998.
4. Lyles, K.W., Gold, D.T., Shipp, K.M., Pieper, C.F., Martinez, S., and Mulhausen, P.L. Association of osteoporotic vertebral compression fractures with impaired functional status. Am J Med **94,** 595, 1993.
5. Cauley, J.A., Thompson, D.E., Ensrud, K.C., Scott, J.C., and Black, D. Risk of mortality following clinical fractures. Osteoporos Int **11,** 556, 2000.
6. Schlaich, C., Minne, H.W., Bruckner, T., Wagner, G., Gebest, H.J., Grunze, M., Ziegler, R., and Leidig-Bruckner, G. Reduced pulmonary function in patients with spinal osteoporotic fractures. Osteoporos Int **8,** 261, 1998.
7. Moerman, E.J., Teng, K., Lipschitz, D.A., and Lecka-Czernik, B. Aging activates adipogenic and suppresses osteogenic programs in mesenchymal marrow stroma/stem cells: the role of PPAR-gamma2 transcription factor and TGF-beta/BMP signaling pathways. Aging Cell **3,** 379, 2004.
8. Egermann, M., Schneider, E., Evans, C.H., and Baltzer, A.W. The potential of gene therapy for fracture healing in osteoporosis. Osteoporos Int **16 Suppl 2,** S120, 2005.
9. Robinson, Y., and Olerud, C. Vertebroplasty and kyphoplasty—a systematic review of cement augmentation techniques for osteoporotic vertebral compression fractures compared to standard medical therapy. Maturitas **72,** 42, 2012.
10. Cloft, H.J., and Jensen, M.E. Kyphoplasty: an assessment of a new technology. AJNR Am J Neuroradiol **28,** 200, 2007.
11. Robinson, Y., Heyde, C.E., Forsth, P., and Olerud, C. Kyphoplasty in osteoporotic vertebral compression fractures—guidelines and technical considerations. J Orthop Surg Res **6,** 43, 2011.
12. Taylor, R.S., Fritzell, P., and Taylor, R.J. Balloon kyphoplasty in the management of vertebral compression fractures: an updated systematic review and meta-analysis. Eur Spine J **16,** 1085, 2007.
13. Deramond, H., Wright, N.T., and Belkoff, S.M. Temperature elevation caused by bone cement polymerization during vertebroplasty. Bone **25,** 17S, 1999.
14. Nussbaum, D.A., Gailloud, P., and Murphy, K. A review of complications associated with vertebroplasty and kyphoplasty as reported to the Food and Drug Administration medical device related web site. J Vasc Interv Radiol **15,** 1185, 2004.
15. Fribourg, D., Tang, C., Sra, P., Delamarter, R., and Bae, H. Incidence of subsequent vertebral fracture after kyphoplasty. Spine **29,** 2270, 2004.
16. Le Nihouannen, D., Daculsi, G., Saffarzadeh, A., Gauthier, O., Delplace, S., Pilet, P., and Layrolle, P. Ectopic bone formation by microporous calcium phosphate ceramic particles in sheep muscles. Bone **36,** 1086, 2005.
17. Heo, H.D., Cho, Y.J., Sheen, S.H., Kuh, S.U., Cho, S.M., and Oh, S.M. Morphological changes of injected calcium phosphate cement in osteoporotic compressed vertebral bodies. Osteoporos Int **20,** 2063, 2009.

18. Zhang, X., Zara, J., Siu, R.K., Ting, K., and Soo, C. The role of NELL-1, a growth factor associated with craniosynostosis, in promoting bone regeneration. J Dent Res **89,** 865, 2010.
19. Aghaloo, T., Cowan, C.M., Chou, Y.F., Zhang, X., Lee, H., Miao, S., Hong, N., Kuroda, S., Wu, B., Ting, K., and Soo, C. Nell-1-induced bone regeneration in calvarial defects. Am J Pathol **169,** 903, 2006.
20. Li, W., Lee, M., Whang, J., Siu, R.K., Zhang, X., Liu, C., Wu, B.M., Wang, J.C., Ting, K., and Soo, C. Delivery of lyophilized Nell-1 in a rat spinal fusion model. Tissue Eng Part A **16,** 2861, 2010.
21. Siu, R.K., Lu, S.S., Li, W., Whang, J., McNeill, G., Zhang, X., Wu, B.M., Turner, A.S., Seim, H.B., 3rd, Hoang, P., Wang, J.C., Gertzman, A.A., Ting, K., and Soo, C. Nell-1 protein promotes bone formation in a sheep spinal fusion model. Tissue Eng Part A **17,** 1123, 2011.
22. Lu, S.S., Zhang, X., Soo, C., Hsu, T., Napoli, A., Aghaloo, T., Wu, B.M., Tsou, P., Ting, K., and Wang, J.C. The osteoinductive properties of Nell-1 in a rat spinal fusion model. Spine J **7,** 50, 2007.
23. Li, W., Zara, J.N., Siu, R.K., Lee, M., Aghaloo, T., Zhang, X., Wu, B.M., Gertzman, A.A., Ting, K., and Soo, C. Nell-1 enhances bone regeneration in a rat critical-sized femoral segmental defect model. Plast Reconstr Surg **127,** 580, 2011.
24. Riew, K.D., Wright, N.M., Cheng, S., Avioli, L.V., and Lou, J. Induction of bone formation using a recombinant adenoviral vector carrying the human BMP-2 gene in a rabbit spinal fusion model. Calcif Tissue Int **63,** 357, 1998.
25. Poynton, A.R., and Lane, J.M. Safety profile for the clinical use of bone morphogenetic proteins in the spine. Spine **27,** S40, 2002.
26. Haid, R.W., Jr., Branch, C.L., Jr., Alexander, J.T., and Burkus, J.K. Posterior lumbar interbody fusion using recombinant human bone morphogenetic protein type 2 with cylindrical interbody cages. Spine J **4,** 527, 2004.
27. Shields, L.B., Raque, G.H., Glassman, S.D., Campbell, M., Vitaz, T., Harpring, J., and Shields, C.B. Adverse effects associated with high-dose recombinant human bone morphogenetic protein-2 use in anterior cervical spine fusion. Spine **31,** 542, 2006.
28. Smucker, J.D., Rhee, J.M., Singh, K., Yoon, S.T., and Heller, J.G. Increased swelling complications associated with off-label usage of rhBMP-2 in the anterior cervical spine. Spine **31,** 2813, 2006.
29. Parfitt, A. M. et al. Bone histomorphometry: standardization of nomenclature, symbols, and units. Report of the ASBMR Histomorphometry Nomenclature Committee. J Bone Miner Res **2,** 595, 1987.
30. Vaidya, R., Carp, J., Sethi, A., Bartol, S., Craig, J., and Les, C.M. Complications of anterior cervical discectomy and fusion using recombinant human bone morphogenetic protein-2. Eur Spine J **16,** 1257, 2007.
31. Tumialan, L.M., Pan, J., Rodts, G.E., and Mummaneni, P.V. The safety and efficacy of anterior cervical discectomy and fusion with polyetheretherketone spacer and recombinant human bone morphogenetic protein-2: a review of 200 patients. J Neurosurg Spine **8,** 529, 2008.
32. Zara, J.N., Siu, R.K., Zhang, X., Shen, J., Ngo, R., Lee, M., Li, W., Chiang, M., Chung, J., Kwak, J., Wu, B.M., Ting, K., and Soo, C. High doses of bone morphogenetic protein 2 induce structurally abnormal bone and inflammation in vivo. Tissue Eng Part A **17,** 1389, 2011.
33. Shen, J., James, A.W., Zara, J.N., Asatrian, G., Khadarian, K., Zhang, J.B., Ho, S., Kim, H.J., Ting, K., and Soo, C. BMP2-induced inflammation can be suppressed by the osteoinductive growth factor NELL-1. Tissue Eng Part A **19,** 2390, 2013.
34. James, A.W., Pan, A., Chiang, M., Zara, J.N., Zhang, X., Ting, K., and Soo, C. A new function of Nell-1 protein in repressing adipogenic differentiation. Biochem Biophys Res Commun **411,** 126, 2011.
35. James, A.W., Shen, J., Zhang, X., Asatrian, G., Goyal, R., Jiang, L., Bengs, B., Culiat, C.T., Turner, A.S., Seim, H.B., 3rd, Wu, B., Lyons, K., Adams, J.S., Ting, K., and Soo, C. NELL-1 in the treatment of osteoporotic bone loss. Nat Commun **6,** 2015, 7362.
36. Zhang, X., Ting, K., Bessette, C.M., Culiat, C.T., Sung, S.J., Lee, H., Chen, F., Shen, J., Wang, J.J., Kuroda, S., and Soo, C. Nell-1, a key functional mediator of Runx2, partially rescues calvarial defects in Runx2(+/–) mice. J Bone Miner Res **26,** 777, 2011.
37. Bokui, N., Otani, T., Igarashi, K., Kaku, J., Oda, M., Nagaoka, T., Seno, M., Tatematsu, K., Okajima, T., Matsuzaki, T., Ting, K., Tanizawa, K., and Kuroda, S. Involvement of MAPK signaling molecules and Runx2 in the NELL1-induced osteoblastic differentiation. FEBS Lett **582,** 365, 2008.
38. Reid, J.E., Meakin, J.R., Robins, S.P., Skakle, J.M., and Hukins, D.W. Sheep lumbar intervertebral discs as models for human discs. Clin Biomech (Bristol, Avon) **17,** 312, 2002.
39. Turner, A.S. The sheep as a model for osteoporosis in humans. Vet J **163,** 232, 2002.
40. Gaynor, J.S., Monnet, E., Selzman, C., Parker, D., Kaufman, L., Bryant, H.U., Mallinckrodt, C., Wrigley, R., Whitehill, T., and Turner, A.S. The effect of raloxifene on coronary arteries in aged ovariectomized ewes. J Vet Pharmacol Ther **23,** 175, 2000.
41. Zarrinkalam, M.R., Beard, H., Schultz, C.G., and Moore, R.J. Validation of the sheep as a large animal model for the study of vertebral osteoporosis. Eur Spine J **18,** 244, 2009.
42. Karasik, D., Hsu, Y.H., Zhou, Y., Cupples, L.A., Kiel, D.P., and Demissie, S. Genome-wide pleiotropy of osteoporosis-related phenotypes: the Framingham Study. J Bone Miner Res **25,** 1555, 2010.
43. Hu, J., Hou, Y., Park, H., and Lee, M. Beta-tricalcium phosphate particles as a controlled release carrier of osteogenic proteins for bone tissue engineering. J Biomed Mater Res A **100,** 1680, 2012.
44. Parfitt, A.M., Drezner, M.K., Glorieux, F.H., Kanis, J.A., Malluche, H., Meunier, P.J., Ott, S.M., and Recker, R.R. Bone histomorphometry: standardization of nomenclature, symbols, and units. Report of the ASBMR Histomorphometry Nomenclature Committee. J Bone Miner Res **2,** 595, 1987.
45. Cheung, J.T., Zhang, M., and Chow, D.H. Biomechanical responses of the intervertebral joints to static and vibrational loading: a finite element study. Clin Biomech **18,** 790, 2003.
46. Kuo, C.S., Hu, H.T., Lin, R.M., Huang, K.Y., Lin, P.C., Zhong, Z.C., and Hseih, M.L. Biomechanical analysis of the lumbar spine on facet joint force and intradiscal pres-

sure—a finite element study. BMC Musculoskelet Disord **11,** 151, 2010.
47. Teitelbaum, S.L. Bone resorption by osteoclasts. Science **289,** 1504, 2000.
48. Marie, P.J. Osteoporosis: a disease of bone formation. Medicographia **32,** 10, 2010.
49. Yavropoulou, M.P., and Yovos, J.G. The role of the Wnt signaling pathway in osteoblast commitment and differentiation. Hormones (Athens) **6,** 279, 2007.
50. Laurencin, C., Khan, Y., and El-Amin, S.F. Bone graft substitutes. Expert Rev Med Devices **3,** 49, 2006.
51. Laurie, S.W., Kaban, L.B., Mulliken, J.B., and Murray, J.E. Donor-site morbidity after harvesting rib and iliac bone. Plast Reconstr Surg **73,** 933, 1984.
52. Frodel, J.L., Jr., Marentette, L.J., Quatela, V.C., and Weinstein, G.S. Calvarial bone graft harvest. Techniques, considerations, and morbidity. Arch Otolaryngol Head Neck Surg **119,** 17, 1993.
53. Kaneko, H., Arakawa, T., Mano, H., Kaneda, T., Ogasawara, A., Nakagawa, M., Toyama, Y., Yabe, Y., Kumegawa, M., and Hakeda, Y. Direct stimulation of osteoclastic bone resorption by bone morphogenetic protein (BMP)-2 and expression of BMP receptors in mature osteoclasts. Bone **27,** 479, 2000.
54. Mathis, J.M., Ortiz, A.O., and Zoarski, G.H. Vertebroplasty versus kyphoplasty: a comparison and contrast. AJNR Am J Neuroradiol **25,** 840, 2004.

Address correspondence to:
Chia Soo, MD, FACS
Division of Plastic and Reconstructive Surgery
Departments of Surgery and Orthopaedic Surgery
David Geffen School of Medicine
University of California, Los Angeles
675 Charles E. Young Dr. South
MacDonald Research Laboratory Room 2641A
Los Angeles, CA 90095

E-mail: bsoo@ucla.edu

Kang Ting, DMD, DMedSci
Division of Growth and Development
and Section of Orthodontics
School of Dentistry
University of California, Los Angeles
675 Charles E. Young Dr. South
MacDonald Research Laboratory Room 2641A
Los Angeles, CA 90095

E-mail: kting@dentistry.ucla.edu

Received: May 17, 2016
Accepted: April 25, 2016
Online Publication Date: May 25, 2016